PCCP

View Online
Dynamic Article Links

Cite this: *Phys. Chem. Chem. Phys.*, 2011, **13**, 15810–15820

www.rsc.org/pccp

PAPER

A theoretical and experimental study on translational and internal energies of H_2O and OH from the 157 nm irradiation of amorphous solid water at 90 K†

Stefan Andersson,*[ab] Carina Arasa,[cd] Akihiro Yabushita,*[e] Masaaki Yokoyama,[e] Tetsuya Hama,‡[e] Masahiro Kawasaki,[e] Colin M. Western[f] and Michael N. R. Ashfold[f]

Received 11th April 2011, Accepted 19th July 2011
DOI: 10.1039/c1cp21138b

The photodesorption of H_2O in its vibrational ground state, and of OH radicals in their ground and first excited vibrational states, following 157 nm photoexcitation of amorphous solid water has been studied using molecular dynamics simulations and detected experimentally by resonance-enhanced multiphoton ionization techniques. There is good agreement between the simulated and measured energy distributions. In addition, signals of H^+ and OH^+ were detected in the experiments. These are inferred to originate from vibrationally excited H_2O molecules that are ejected from the surface by two distinct mechanisms: a direct desorption mechanism and desorption induced by secondary recombination of photoproducts at the ice surface. This is the first reported experimental evidence of photodesorption of vibrationally excited H_2O molecules from water ice.

1. Introduction

A number of studies have been performed on the photochemistry of water ice, because of the interest in photodesorption and photodissociation in the fields of atmospheric chemistry[1,2] and astrophysics.[3] Water ice has been observed on bodies in the outer Solar system,[4] *e.g.*, satellites of Jupiter[5] and Saturn[6–8] and Kuiper Belt objects,[9–14] as well as in interstellar and circumstellar regions of space.[15–22] Observational evidence suggests that water ice in the Solar system is mostly crystalline with some smaller amounts of amorphous ice. The balance between the two types of ice is governed by amorphization through irradiation by ions and electrons from the Solar wind and by Solar ultraviolet (UV) photons, and thermal recrystallization, which means that warmer ices are more likely to be crystalline than colder ones given equal radiation intensity.[4,5] A large part of gas phase water in interstellar and circumstellar space has been attributed to photodesorption of water molecules induced by absorption of UV photons at ice-covered grains.[23–25] Interstellar and circumstellar ices are most likely predominantly amorphous, but some crystalline ice may exist, *e.g.*, close to young stellar objects.[22]

Photo-ejection of water molecules from ice surfaces has been investigated in the wavelength range from vacuum ultraviolet (VUV) to the visible region *via* one- and multi-photon absorption, and an energy threshold of ~9 eV identified. Since this value is compatible with the width of the ice band gap,[26] it has been speculated that the observed photo-ejection results from formation of excitons in ice.[27–29] Westley *et al.* investigated the desorption mechanism of H_2O from water ice films by 10.2 eV (Lyman-α) photons.[30,31] The authors suggested that the accumulation and diffusion of photo-produced radicals in/on the ice was necessary for water desorption to occur. Öberg *et al.* reached a different conclusion, however.[32] They used a VUV lamp emitting in the range 7.0–10.5 eV to irradiate ices at surface temperatures in the range 18–100 K and detected desorbing species such as H_2O, OH, H_2 and O_2 as well as determining the composition of the ice, and concluded that desorption of H_2O and OH from the ice occurs mainly *via* primary processes. Since the reaction mechanisms are inferred by identifying photodesorbed products and species formed in/on ice, they were not able to reveal the formation dynamics or finer details of the reactions. In our previous studies, we investigated photodissociation of water in/on amorphous solid water (ASW) at 90 K using pulsed 157 nm laser radiation, *i.e.*, at a wavelength within the first absorption band of the ice, to reveal the translational and

[a] *SINTEF Materials and Chemistry, P.O. Box 4760, 7465 Trondheim, Norway. E-mail: stefan.andersson@sintef.no*
[b] *Department of Chemistry, Physical Chemistry, University of Gothenburg, 41296 Gothenburg, Sweden*
[c] *Leiden Observatory, Leiden University, P. O. Box 9513, 2300 RA Leiden, The Netherlands*
[d] *Leiden Institute of Chemistry, Leiden University, P. O. Box 9502, 2300 RA Leiden, The Netherlands*
[e] *Department of Molecular Engineering, Kyoto University, Kyoto 615-8510, Japan. E-mail: yabushita@moleng.kyoto-u.ac.jp*
[f] *School of Chemistry, University of Bristol, Bristol BS8 1TS, UK*
† This article was submitted as part of a collection following the Low Temperature Spectroscopy/Kuiper Belt Objects symposium at Pacifichem2010.
‡ Present address: Institute of Low Temperature Science, Hokkaido University, Sapporo 060-0819, Japan.

internal energy distributions of OH(v = 0, 1) and H_2O(v = 0).[33–35] The photodesorption of OH and H_2O from the VUV photolysis of ASW was also studied by molecular dynamics (MD) calculations.[36–38] These simulations predicted the existence of the previously unknown "kick-out" mechanism for water photodesorption, whereby an energetic H atom, formed by photodissociation of a molecule in the ice, "kicks" a neighboring molecule out of the surface, often assisted by a repulsive interaction induced by the excitation in the ice.

The desorption mechanisms for H_2O(v = 0) discussed in our previous papers[34,35] can be grouped into three types. These are distinguished on the basis that the desorbing molecule is: (A) the one that experiences the initial electronic excitation, (B) expelled as a result of electronic excitation of a neighboring molecule, or (C) formed by the recombination of photofragments arising from different photodissociated molecules. Types (A) and (B) are considered to be direct processes, whereas (C) involves secondary processes. Initially, type (A) and (C) mechanisms will involve high internal energies in the desorbing molecules (due to photoexcitation and recombination, respectively). Both might thus be expected to favor formation of vibrationally excited H_2O molecules, whereas the type (B) mechanism could well result in desorbed H_2O(v = 0) molecules.

The exact mechanism underpinning type (B) desorption is difficult to specify. Part of the excitation energy is somehow transferred from the surface into translational energy of a H_2O molecule. This could occur *via* an exciton-induced process, either through a repulsive electronic interaction, or by kinetic energy transfer from a vibrationally excited H_2O molecule formed by electronic relaxation to the ground state. The kick-out desorption mechanism is closely related to the exciton-induced process in as much that it also involves a change in the binding properties of the desorbing molecule but, additionally, requires a kick from an incident H atom to ensure desorption. In the electronic relaxation process, the vibrational excitation that promotes desorption comes from de-excitation of the excited state molecule, with the initial electronic energy transformed into nuclear kinetic energy. This can occur "directly", before the molecule has dissociated, or "semi-directly", through dissociation and prompt (geminate) recombination of the resulting photofragments. This semi-direct desorption mechanism was evident in the previous simulations by Andersson and van Dishoeck,[37] albeit with a much lower probability than the other desorption mechanisms. In conclusion, therefore, there are several different detailed mechanisms that could lead to direct photodesorption of H_2O(v = 0) molecules.

Comparison with experiments showed that the measured translational and rotational energy distributions of desorbing H_2O(v = 0) closely matched the energies predicted by the MD simulations for the kick-out mechanism, lending credibility to this as a plausible mechanism for water photodesorption.[34,35] Initially the MD simulations were run only for T = 10 K,[36,37] but in the most recent study[38] the focus was on the temperature dependence of photodesorption in the range T = 10–90 K. It was found that H_2O and OH photodesorption probabilities show a significant dependence on temperature, in qualitative agreement with experiments.[32] The experimental photodesorption yields from D_2O and H_2O ice showed a more pronounced rise with increasing temperature than predicted by the MD simulations. The latter only included direct photodesorption caused by absorption of a single VUV photon in the ice and thus did not allow for secondary processes (which must involve multiple excitations). Thus it was suggested that the increased desorption induced yields at higher temperatures might be associated with secondary recombination of photoproduced H and OH radicals, which will have higher mobility at higher temperatures.

The present work describes further advanced experimental studies and additional classical MD calculations of the translational and rotational energies of H_2O and OH species desorbing from an ASW ice surface exposed to 157 nm laser radiation. A small part of the results have been presented before,[34,35] but are repeated here to add context. The new MD results presented in this paper are translational energy distributions of the H_2O molecules photodesorbed by the kick-out mechanism and by the direct recombination mechanism, as well as energy distributions of desorbing OH(v = 0 and 1). We also report a previously undetected photodesorption component evident through the experimental detection of H^+ and OH^+ signals, which we propose as a signature of highly vibrationally excited H_2O molecules. Comparison with our previous experimental results and the new detection of H^+ and OH^+ signals provide new insights into the prevailing reaction mechanisms and dynamics.

2. Molecular dynamics simulations

Details of the MD calculations of ice photochemistry have been described elsewhere.[36–38] Here we mostly focus on what is different from the previous calculations. To obtain a realistic model of the experimental setup, we have created an amorphous ice surface by rapidly cooling a liquid water surface from 300 K to 90 K, in the manner described by Al-Halabi *et al.*[39,40] and Andersson *et al.*[36] Initially, a periodic slab of the equivalent of 8 crystalline bilayers was created with 480 molecules in each periodic cell. Out of these molecules, 120 were kept frozen at all times to simulate bulk ice. The remaining, fully mobile, 360 molecules were divided into 12 monolayers of 30 molecules each. The monolayers are defined as the equivalent of half a bilayer of crystalline ice.[36]

All molecules are initially treated as rigid rotors and their interactions are treated with the TIP4P potential.[41] One molecule is selected for photoexcitation and this molecule is then made completely flexible. The excitation model uses a Monte Carlo sampling over a Wigner distribution of the ground vibrational state of H_2O[36] and the sampled geometries are projected from the electronic ground state to the first excited state potential energy surface (PES). The latter is based on the PES of the first excited state of gas phase H_2O,[42–44] combined with modified partial charges on the excited molecule. The partial charges were set as atom-based charges of $-0.2e$ for O and $0.1e$ for H.[36] This adjustment was made so as to obtain the best fit to the peak of the experimental UV absorption spectrum of ice previously reported by Kobayashi.[45] The excitation energy was calculated as the energy difference between the sampled configuration in the

excited state and the ground state. For initial conditions, we have selected only those excitation energies that lie in the 7.8–8.0 eV range (corresponding to wavelengths between 155 and 159 nm).

Photodesorption of OH and H_2O from amorphous ice at 10 K was found to be insignificant following excitation of molecules below the third monolayer, so we have focused attention on excitations within the top three layers of the ice. All molecules in these top three monolayers have been chosen for photoexcitation, one molecule at a time. We only consider the absorption of a single photon in these simulations.

For each molecule, 10 000 initial configurations were created by the sampling procedure outlined above. From the resulting 900 000 configurations, about 70 000 were found to lie in the 7.8–8.0 eV excitation energy range and were thus used to initiate the trajectories in this study. The trajectories were run until the photofragments (H and OH), a recombined H_2O molecule, or another (rigid) H_2O had desorbed or were accommodated to the ice surface. Desorption was defined as occurring when the atom or molecule of interest was at a distance where it was practically non-interacting with the ice surface, *i.e.* 10 Å above the surface in this case. Accommodation was considered to be complete when the translational energy of H, OH and/or H_2O is below $k_B T_{surf}$ and the binding energy to the surface is 2, 10, and 30 kJ mol^{-1}, respectively.

If desorption occurred, the energy distribution of the desorbing species was analyzed. The translational energies were monitored for all species, as well as the rotational energies for OH and desorbing rigid H_2O, vibrational energies for OH, and total internal energies for recombined H_2O. The recombined H_2O molecules were found to be so highly vibrationally excited that the separation of rotational and vibrational degrees of freedom became impractical. Translational energies of OH and H_2O were sorted in 0.05 eV wide bins to obtain translational energy distributions and to estimate the corresponding translational temperature, T_{trans}. The vibrational energies of OH were binned to the closest vibrational quantum state in energy, thereby yielding a population distribution over vibrational quantum state. Note that this analysis does not invoke explicit quantum mechanics, only a consideration of vibrational energies. The error bars associated with the calculated results all correspond to a 95% confidence interval.

3. Experimental

Photodesorption studies of OH and H_2O from ice films at 90 K were carried out in a high vacuum chamber equipped with two turbo-molecular pumps in tandem and two pulsed valves, using an excimer laser and a dye laser. The experimental details are described elsewhere.[46] In brief, the vacuum chamber was evacuated to a base pressure of 10^{-8} Torr. An optically flat sapphire substrate, sputter coated with a thin film of Au, was supported in the center of the chamber by a liquid-nitrogen-cooled manipulator. ASW films were prepared by back-filled deposition of water vapor onto the substrate at 90 K for 60 min, using a pulsed valve (General Valve) operating at 10 Hz with stagnation pressure of H_2O vapor of 20 Torr. A flat plate was attached in front of the pulsed valve to diffuse vapors throughout the chamber. The exposure was typically 1800 L (1 L = 1×10^{-6} Torr s) of gaseous water, which resulted in the formation of 600 monolayers of H_2O on the Au substrate.[47]

An F_2 excimer laser (Lambda Physik, 10 Hz, OPTexPro) at 157 nm was used as the pulsed light source for photodesorption. The incident fluence was typically < 0.1 mJ cm^{-2} $pulse^{-1}$ at 157 nm in a 15 ns pulse duration (corresponding to an incident intensity ~ 7 kW cm^{-2}). The OH photofragments were ionized by 2 + 1 resonance-enhanced multiphoton ionization (REMPI) *via* the $D^2\Sigma^-(v = 0) \leftarrow X^2\Pi(v = 0)$ transition at 243.5–244.5 nm and *via* the $D^2\Sigma^-(v = 1) \leftarrow X^2\Pi(v = 0)$ and $3^2\Sigma^-(v = 0) \leftarrow X^2\Pi(v = 1)$ transitions at 237.5–237.7 nm, using the focused ($f = 0.10$ m lens) frequency doubled output of an Nd^{3+}:YAG pumped dye laser. Two-photon absorption cross sections reported by Greenslade *et al.* allow estimation of the $(v'' = 1)/(v'' = 0)$ ratio.[48] Photodesorbed water molecules were detected by 2 + 1 REMPI of H_2O on the C(000)–X(000) transition in the wavelength range 247.5–248.5 nm using the focused ($f = 0.10$ m lens) frequency doubled output of an Nd^{3+}:YAG pumped dye laser. Non-resonant multiphoton excitation spectra for forming H^+ and OH^+ ions were measured at longer wavelengths (in the ranges 251.8–253.8 nm and 257.4–260.1 nm) appropriate for the C–X $\Delta v_2 = -1$ and $\Delta v_2 = -2$ and/or $\Delta v_1 = -1$ transitions, respectively. These ion signals were detected by a small mass spectrometer. The flight distance between the substrate and the detection region was set to 2 mm. REMPI signal intensities were taken as a function of time delay, t, between the photolysis and probe laser pulses, which corresponds to the flight time between the substrate and the REMPI detection region. The time-of-flight (TOF) spectra were fitted to the flux-weighted Maxwell–Boltzmann (M–B) distribution defined by a translational temperature, T_{trans}.[49]

4. Results

4.1 UV absorption of water ice

Given the potential used in the present MD calculations, we predict that most of the molecules excited at 157 nm are very close to the vacuum interface: of the configurations sampled with excitation energies 7.8–8.0 eV, about half (49%) are in the top monolayer, 34% in the second and 17% in the third monolayer. Since most photodesorption occurs when the excitation is in the top monolayers,[36–38] excitations in this energy range should lead to a high probability of photodesorption. Support for this view is provided by previous simulations showing that the H atom photodesorption probability per absorbed photon declines with increasing excitation energy—because lower energy excitations are concentrated in the top layers.[37]

4.2 Photodesorption of H_2O molecules

4.2.1 Molecular dynamics. The MD calculations show two distinct mechanisms of H_2O photodesorption. One is the direct recombination mechanism, where the photodissociation

products H and OH recombine instantly and subsequently desorb. The other is where a neighboring H_2O molecule is "kicked out" by momentum transfer from an energetic H atom produced from photodissociation. The efficiency of this momentum transfer is in many cases boosted by interactions between the photoexcited H_2O and a photoproduced proximate OH species.[38] This leads to a repulsive potential for the neighboring ground-state H_2O which, as a result, gains translational energy. The subsequent momentum kick from the H atom supplies sufficient energy for the molecule to desorb. Since all H_2O molecules (except the one that is photoexcited) are kept internally rigid in the simulations, there is of course no possibility of energy transfer from the H atom to the intramolecular degrees of freedom of the kicked-out H_2O molecule. This means that all kicked-out molecules in these simulations are considered to remain in their vibrational ground state throughout the trajectory.

The simulated H_2O photodesorption probability was found to be 8×10^{-3} per absorbed UV photon. Of these, ~25% were kicked out and the rest were recombined molecules. The mean translational energy $\langle E_{trans} \rangle$ of the kicked-out molecules was 0.25 ± 0.03 eV, which would correspond to a translational temperature, $T_{trans} = 1450 \pm 150$ K, calculated by using $\langle E_{trans} \rangle = 2k_B T_{trans}$. The mean rotational energy $\langle E_{rot} \rangle$ was 0.039 ± 0.006 eV, corresponding to $T_{rot} = 300 \pm 50$ K ($\langle E_{rot} \rangle = 3/2k_B T_{rot}$). These results compare favorably with the previously reported experimental energy distributions for desorbing $H_2O(v = 0)$, as can be seen from Table 1.[34,35] The simulated translational energies are at the low end, but still within the experimental error bars, while the mean rotational energies show perfect agreement. The simulated translational energy distribution is quite close to the thermal distribution at 1450 K (Fig. 1), within the error bars, suggesting that this desorption process follows the behavior predicted by Zimmermann and Ho[49] for particles desorbing on a repulsive potential. *A priori*, it was not clear that the simulated energies would agree with a M–B energy distribution, so this finding serves to reinforce the agreement with experiments.

The predicted energy distributions of H_2O molecules formed by recombination and subsequent desorption are very different. The predicted translational energy distribution is a little hotter, with $\langle E_{trans} \rangle = 0.34$ eV, which equates to $T_{trans} \sim 2000$ K. The average rovibrational energy, however, is very much hotter—close to the H + OH dissociation limit (*i.e.* 5.3 eV above the minimum on the H_2O PES). Even the least excited H_2O molecules formed by this mechanism are predicted to have an internal energy of ~1.8 eV (relative to the vibrational ground state). This mechanism is thus predicted to yield H_2O molecules with very high levels of internal excitation (henceforth denoted as $H_2O(v^*)$), and no

Table 1 Translational and rotational temperatures of photodesorbed ($\lambda = 157$ nm) $H_2O(v = 0)$ molecules from amorphous solid water at 90 K

	T_{trans} (K)	T_{rot} (K)
Experimental[a]	1800 ± 500	300 ± 100[b]
MD calculations	1450 ± 150	300 ± 50

[a] Ref. 34 and 35. [b] Determined for a time of flight of 2.5 μs.

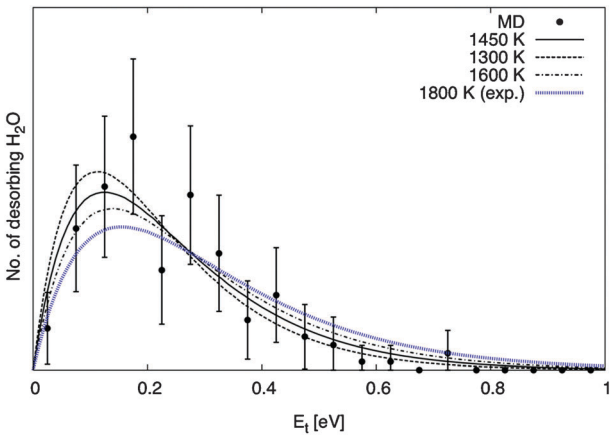

Fig. 1 Translational energy distribution of the H_2O molecules photodesorbed by the kick-out mechanism in the MD calculations. The desorption energies have been binned into 0.05 eV wide intervals. The error bars correspond to a 95% confidence interval. Maxwell–Boltzmann distributions corresponding to the average translational energy (with upper and lower error limits) are included as well as the experimentally obtained distribution for $H_2O(v = 0)$ molecules.

$H_2O(v = 0)$ products. The calculated translational energy distribution shown in Fig. 2 does not quite match to a M–B distribution—reinforcing the view that the $H_2O(v = 0)$ molecules observed experimentally do not arise from this mechanism.

4.2.2 Experimental detection. We tried to detect $H_2O(v^*)$ molecules by 2 + 1 REMPI *via* the C state. The possibilities for this are, however, limited both by the properties of the C state and the spectroscopic information available. The behavior of the vibrationless level of the C state is well understood (see ref. 50 and 51), with all levels predissociated to a degree that depends strongly on J and K_a. The available information on vibrationally excited levels of the C state is very sparse, but the limited information available[52] indicates even stronger

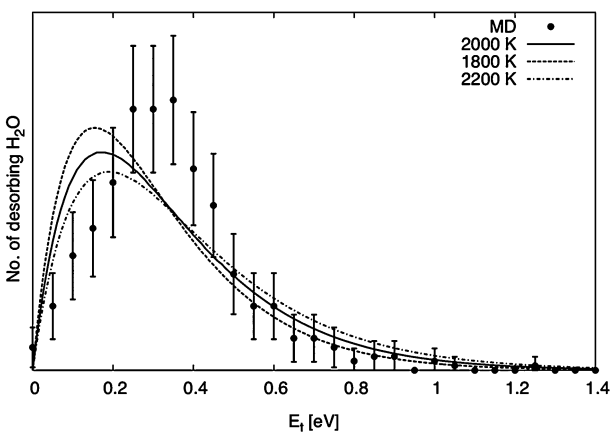

Fig. 2 Translational energy distribution of the H_2O molecules photodesorbed by the direct recombination mechanism in the MD calculations. The desorption energies have been binned into 0.05 eV wide intervals. The error bars correspond to a 95% confidence interval. Maxwell–Boltzmann distributions corresponding to the average translational energy (with upper and lower error limits) are included.

predissociation, depending on the vibrational state. The reported 2 + 1 REMPI spectra are thus dominated by transitions involving C state levels with low J' and $K_a' \sim 0$. The X and C states of H_2O, and the ground state of H_2O^+, all have similar equilibrium geometries (and vibrational frequencies). On Franck–Condon grounds, therefore, we can expect that the H_2O(C–X) transition would be dominated by diagonal (*i.e.* $\Delta v = 0$) excitations, and that $H_2O(v^*)$ molecules would give REMPI signals in the same spectral region as the C(000)–X(000) origin band. All of the prominent features in this region of the 2 + 1 REMPI spectrum recorded in the present study by monitoring the parent ion are attributable to $H_2O(v = 0)$ molecules, but some weak H^+ and OH^+ signals were observed, with a different spectral signature to that of the $H_2O(v = 0)$ molecules. This is not particularly surprising—reflecting (i) the relative efficiency of the kick-out mechanism for forming $H_2O(v = 0)$ molecules and (ii) the (relative) stability of the resonance enhancing C(000) level with respect to predissociation.[53,54] The observation of fragment ions, with a different spectral signature to that of the $H_2O(v = 0)$ molecules, could be due to REMPI of $H_2O(v^*)$ molecules rather than direct ionization of neutral H or OH fragments.

To explore this possibility further, we focused attention on spectral regions appropriate for $\Delta v_2 = -1$ and $\Delta v_1 = -1$ transitions, *i.e.* around the expected position for C(000)–X(010), and C(000)–X(100) transitions. The latter region also covers the expected region for $\Delta v_2 = -2$ transitions as the $v_1 = 1$ and $v_2 = 2$ levels of H_2O are close in energy. Structured excitation spectra for forming both H^+ and OH^+ ions were observed in both regions, but the corresponding spectrum for forming ions with m/z 18 (H_2O^+) was weak and devoid of structure. Simulations of transitions involving C(000) in this region can easily be produced as the constants for both upper and lower states are readily available. Fig. 3 shows a simulation of the $\Delta v_2 = -1$ region calculated using PGOPHER[55] together with spectroscopic parameters taken from the literature as described in ref. 50 assuming a Boltzmann distribution over rotational states with T_{rot} = 350 K. It is clear from the figure that, while the density of features is not unreasonable, there is no clear match with the calculated 2 + 1 REMPI spectrum of the H_2O C(000)–X(010) transition. Similar simulations of the 000–100 and 000–020 bands also gave no direct match with experiment. It is not possible to simulate transitions from excited vibrational states (*e.g.* $0(n-1)0$–$0n0$ or $(m-1)00$–$m00$)) as the relevant C state constants and predissociation rates are not known. We would expect such transitions to be broadly similar, but with fewer sharp lines as levels with higher J' or K_a' are more likely to predissociate giving a broad background to the spectrum.

The evident disagreement between the measured H^+ and OH^+ yield spectra and the H_2O C(000)–X(010) 2 + 1 REMPI spectrum is consistent with the results of the MD simulations, which predict that the $H_2O(v^*)$ molecules formed by the recombination/desorption mechanism have internal energies > 1.8 eV and, on average, ~5.3 eV (*cf.* the ~0.2 eV vibrational energy associated with the $v_2 = 1$ level). Such molecules would be expected to follow the excitation scheme:

$$H_2O(v^*) + 2h\upsilon \rightarrow H_2O(C,v^*) \qquad (1)$$

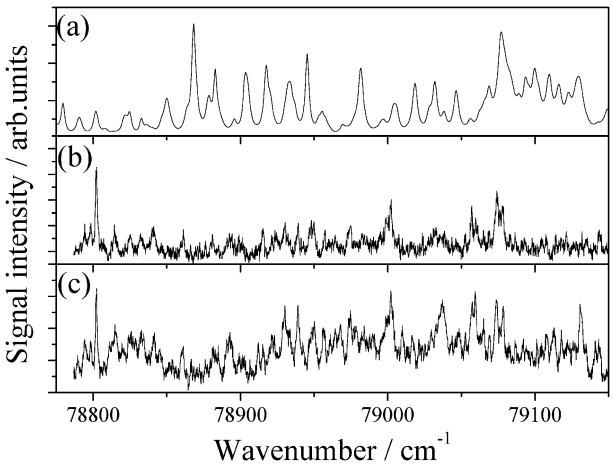

Fig. 3 (a) Simulated REMPI excitation spectrum of H_2O, resonance enhanced at the two photon energy *via* the C(000)–X(010) transition, assuming spectroscopic and predissociation parameters from the literature (as described in ref. 50) and a Boltzmann rotational state population distribution with T_{rot} = 350 K. Action spectra for forming (b) H^+ and (c) OH^+ fragment ions by 157 nm photoirradiation of ASW (time-of-flight = 2.0 μs).

Many of the $H_2O(C,v^*)$ molecules will predissociate to neutral H atoms and OH radicals at this stage but, in the presence of the intense REMPI laser radiation, some will absorb another photon and ionise, *i.e.*

$$H_2O(C,v^*) + h\upsilon \rightarrow H_2O^+(X,v^*) \qquad (2)$$

Given the similar equilibrium geometries of the C state and the ion, we assume that the parent vibrational excitation is broadly conserved upon ionisation. The bond dissociation energies, $D_0(H\text{–}OH^+)$ and $D_0(H^+\text{–}OH)$ are 5.500 eV and 6.082 eV, respectively,[56] so absorption of one further REMPI laser photon would suffice to yield the observed H^+ and OH^+ fragment ions, for all but the lowest few vibrational levels of H_2O^+ *i.e.*

$$H_2O^+(X,v^*) + h\upsilon \rightarrow H^+ + OH$$
$$\rightarrow OH^+ + H \qquad (3)$$

Any parent ions formed *via* steps (1) and (2) would be expected to show the spectral signature of the initial C–X excitations, but the parent ion yield is small—presumably because the further one photon step (3) has high probability at the prevailing laser intensities. We can therefore understand the observed H^+ and OH^+ fragment ion signals as originating from photodissociation of H_2O^+ ions in a wide range of vibrational states, with no clear match with the spectral of simulations as only a few peaks from a few vibronic bands involving $H_2O(v^*)$ molecules give sharp peaks.

Fig. 4 shows typical TOF spectra of H^+ and OH^+, which are very similar to each other. The obvious temporal and spectral similarities of the H^+ and OH^+ signals support the view that both originate from a common species (photodesorbed $H_2O(v^*)$ molecules). Given this assumption, the H^+ and OH^+ TOF spectra in Fig. 4 are characterized by T_{trans} = 10 000 ± 2000 K ($\langle E_{trans}\rangle$ = 1.73 ± 0.34 eV) and 1800 ± 300 K ($\langle E_{trans}\rangle$ = 0.31 ± 0.05 eV) for the fast and slow components, respectively.

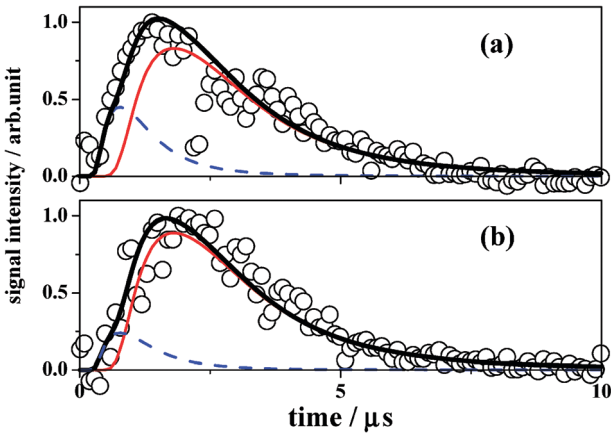

Fig. 4 Time-of-flight spectra of (a) H^+ and (b) OH^+ fragment ions from vibrationally excited H_2O molecules formed by 157 nm photo-irradiation of ASW at 90 K following excitation in the region of the H_2O(C–X) $\Delta v_2 = -1$ transitions. The solid curves are fits to the data derived assuming Maxwell–Boltzmann translational energy distributions for the parent water molecule with T_{trans} = 10 000 K (broken blue line) and 1800 K (red line).

The time evolution curves of H^+ and OH^+ signals from the $H_2O(v^*)$ molecules excited in the region of the C–X $\Delta v_2 = -1$ transition were measured as a function of 157 nm irradiation time for the TOF components at t = 0.5 and 3.0 μs, as shown in Fig. 5. The H^+ and OH^+ signals at t = 3.0 μs appeared promptly and thereafter remained constant, while those at t = 0.5 μs gradually increased but reached a limiting value after several thousand laser shots.

4.3 Photodesorption of OH

The calculated probability for photodesorption of OH is 1.6% per absorbed UV photon. Almost all of the desorbing OH originates in the top two monolayers, 72% from the top monolayer, 27% from the second, and only 0.2% from the third monolayer. 73 ± 3% of the photodesorbed OH radicals are predicted to be formed in their vibrational ground state, with ~17% in v = 1, 6% in v = 2, and the remaining 4% in higher levels ($v \leq 6$). This gives a $N(v = 1)/N(v = 0)$ population ratio of 0.24 ± 0.04 (Table 2), which compares well with the experimentally obtained value (0.30 ± 0.05). The predicted $N(v = 2)/N(v = 0)$ population ratio is just 0.08 ± 0.02. No OH(v = 2) desorption products have been observed experimentally; whether this indicates a real discrepancy between experiment and simulation, or simply reflects signal to noise considerations in the former, is unclear.

For OH(v = 0), the simulated $\langle E_{trans} \rangle$ is 0.29 ± 0.01 eV, which corresponds to T_{trans} = 1700 ± 100 K (Table 2). The translational energy distribution is quite close to a M–B distribution (see Fig. 6), but somewhat hotter than the experimentally measured distribution (T_{trans} = 1300 ± 200 K). The simulated rotational temperature is 480 ± 50 K, which is in good agreement with the experimental value 400 ± 100 K.[33] As shown in Table 2 and Fig. 7, the simulated translational temperature of the OH(v = 1) products (1350 ± 150 K) accords well with the corresponding experimental value (1300 ± 200 K), but the calculated rotational temperature is somewhat higher (520 ± 120 K, *cf.* the experimental value of 300 ± 100 K).

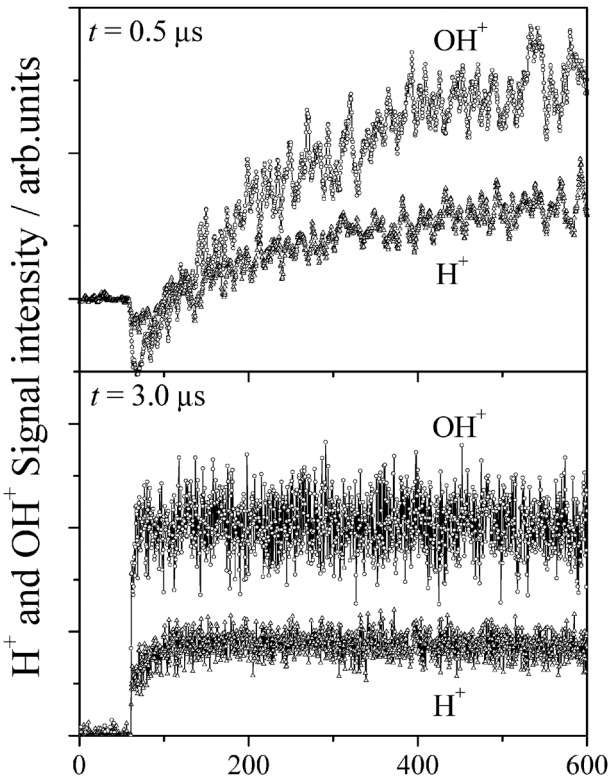

Fig. 5 Time evolution curves of the H^+ (lower curve in each plot) and OH^+ (upper curve) signals attributed to vibrationally excited H_2O molecules following excitation in the region of the H_2O(C–X) $\Delta v_2 = -1$ transitions at t = 0.5 μs (adjacent averaging smoothing of 10 points) and 3.0 μs (raw data) as a function of the 157 nm irradiation time.

5. Discussion

The energy distributions found experimentally and predicted by the MD simulations are generally in good agreement. This is quite remarkable, given that the only adjustable parameter in the set-up of the simulations was the distribution of partial charges in the photoexcited H_2O molecule[36]—which was chosen to make the maxima of the calculated and experimental UV absorption spectra coincide. All other potentials were kept as initially derived by *ab initio* calculations or, as in the case of the TIP4P potential, based on empirical data for liquid water. The dynamical approximations, rigid H_2O molecules and the use of classical dynamics, also seem to be reasonable in light of the results presented here. We recognize, however, that for other observable properties it will likely be necessary to perform more advanced simulations.

5.1 H_2O photodesorption

The present experiments successfully monitor $H_2O(v = 0)$ molecules *via* H_2O^+ detection, and the signals from H^+ and OH^+ additionally suggest the presence of H_2O molecules with significant vibrational excitation. As discussed in the Introduction, and as shown by the MD simulations, vibrationally

Table 2 Translational and rotational temperatures of OH (v = 0,1) products from the 157 nm photoexcitation of ASW and their relative yields, and a comparison with the available gas phase quantities

	OH(v = 0)		OH(v = 1)		Population ratio
	T_{trans} (K)[a]	T_{rot} (K)	T_{trans} (K)[a]	T_{rot} (K)	$N(v = 1)/N(v = 0)$
ASW	7500 ± 1000 (5%) 1300 ± 200 (95%)	400 ± 100[b]	7500 ± 1000 (10%) 1300 ± 200 (90%)	300 ± 100[b]	0.30 ± 0.05
MD calculations	1700 ± 100	480 ± 50	1350 ± 150	520 ± 120	0.24 ± 0.04
H_2O (gas phase)[c]	1200	600	—	450	1.06–1.11[d]

[a] Numbers in the parentheses are the contribution of each TOF component. [b] Determined for a time of flight of 1.5 μs. [c] Ref. 62. [d] Ref. 64.

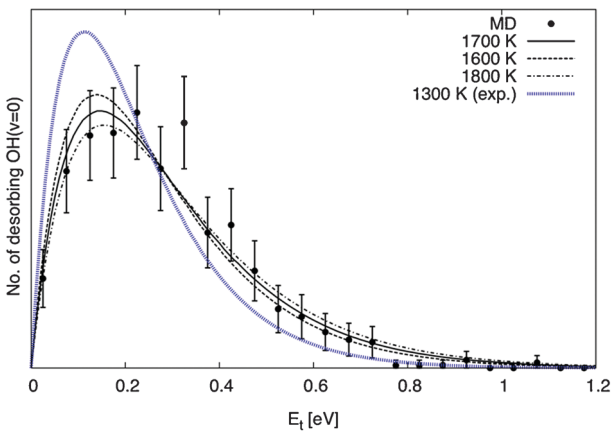

Fig. 6 Translational energy distribution of OH(v = 0) products returned by the MD calculations. The desorption energies have been binned into 0.05 eV wide intervals. The error bars correspond to a 95% confidence interval. Maxwell–Boltzmann distributions corresponding to the average translational energy (with upper and lower error limits) are included as well as the experimentally obtained distribution.

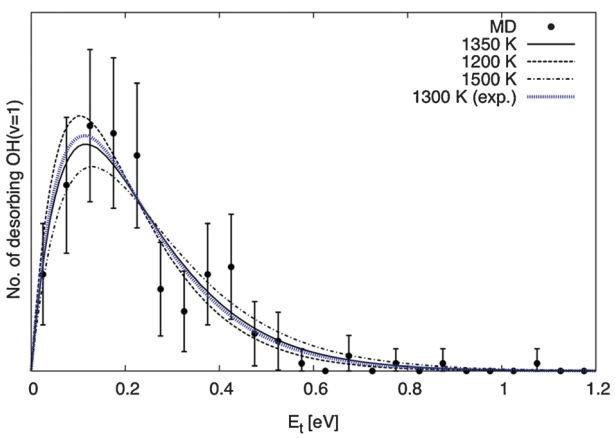

Fig. 7 Translational energy distribution of OH(v = 1) products returned by the MD calculations. The desorption energies have been binned into 0.05 eV wide intervals. The error bars correspond to a 95% confidence interval. Maxwell–Boltzmann distributions corresponding to the average translational energy (with upper and lower error limits) are included as well as the experimentally obtained distribution.

excited H_2O molecules can arise *via* more than one desorption mechanism. Both type (A) and type (C) mechanisms are expected to favor formation of vibrationally excited H_2O molecules, as a result of desorption induced by photoexcitation and photofragment recombination, respectively.

For the mechanism of type (A), our MD calculations provide internal energy distributions of desorbing H_2O molecules produced by the near-instantaneous geminate recombination of H and OH fragments formed by the photodissociation of a single H_2O molecule. These molecules are found to carry a large amount of vibrational excitation, with average internal energies equal to the dissociation energy of H_2O. We find no evidence for $H_2O(v = 0)$ molecules arising from this desorption mechanism. The simulated internal energy of desorbing recombined H_2O molecules most likely represents an upper limit to what would be observed in experiments. In the MD simulations, the recombined molecules are allowed to exchange energy with translational and rotational (librational) modes of the surrounding molecules, but not to the internal vibrational modes, as the other molecules are restricted to be internally rigid (see preliminary H–H_2O collision study reported below). The MD calculations also predict translational energy distributions that do not quite follow a single M–B distribution.

An alternative form of photoinduced desorption is the recombination of H and OH produced from photodissociation of different molecules in the ice (a secondary, type (C) process). Recombination of OH and OH could also yield H_2O molecules. The energy distributions of these desorbing molecules would probably differ somewhat from those produced directly upon photodissociation, since the fragments involved in the secondary recombination would have lost much of their initial translational energies, and would thus need to release more of the recombination energy in order to desorb than in the case of direct desorption, where the fragments still carry most of the initial translation energy. Therefore, one might expect cooler rovibrational energy distributions from this secondary process than from the direct recombination.

Whether these two different populations of desorbing recombined molecules would be discernible in experimental measurements is not clear. However, we might anticipate differences in the time evolution of desorbing molecules arising as a result of geminate and secondary recombination. Under the present experimental conditions geminate (type (A)) recombination would be fairly constant with time, while secondary (type (C)) recombination would increase with time as increasing amounts of reactive radicals are formed and accumulated in the ice. Recalling the time evolution of the signals in Fig. 5, it seems likely that the translationally hot component of the signal we associate with desorbing $H_2O(v^*)$

molecules is due to secondary recombination and that the cooler component is due to direct recombination. It would be helpful to have data from MD simulations to resolve the mechanisms involved in secondary recombination, but the present MD simulations cannot predict the outcome of secondary processes. The recombination-induced desorption that is found in the simulations is due to the recombination of fragments originating from the same H_2O molecule (*i.e.* geminate recombination). A different set of simulations would need to be run, in which, for example, translationally cool H and OH recombine at the surface and possibly desorb by transforming internal energy to translational energy.

The action spectra for forming H^+ and OH^+ ions following two photon excitation in the region of the C–X $\Delta v_2 = -1$ and $\Delta v_1 = -1$ transitions were similar, consistent with the proposed excitation Scheme (1)–(3). The TOF spectra of these H^+ and OH^+ fragment ions both consist of two components with $H_2O(v^*)$ translational temperatures of 10 000 K ($\langle E_{trans} \rangle$ = 1.73 eV) and 1800 K ($\langle E_{trans} \rangle$ = 0.31 eV), respectively. To explore the origin of the H^+ and OH^+ signals further, the H^+ and OH^+ signals formed when exciting in the region of the C–X $\Delta v_2 = -1$ transitions at t = 0.5 μs (probing the T_{trans} = 10 000 K component) and at 3.0 μs (for the T_{trans} = 1800 K component) were measured as a function of 157 nm irradiation time, as shown in Fig. 5. The T_{trans} = 1800 K products appeared promptly, while those with T_{trans} = 10 000 K gradually increased over time. The TOF spectrum of desorbing $H_2O(v = 0)$ molecules is also dominated by a T_{trans} = 1800 K component which, again, appears promptly.[35] Thus we need to consider if the corresponding component of the H^+ and OH^+ signals in Fig. 5 could be due to the kick-out of vibrationally excited H_2O, since it is quite probable that energy is also transferred to vibrational modes of the kicked-out molecule. This possibility is "switched off" in our MD simulations due to the imposed rigidity of the molecules in the ice; thus we cannot rule out vibrational excitations on the basis of our simulations. Nonetheless, we only expect relatively modest levels of vibrational excitation in products arising *via* the kick-out mechanism (see below) and, on that basis, we would have expected rather better agreement between the measured and simulated spectra originating from $H_2O(v = 1)$, as discussed in section 4.2. Following the discussion in the previous paragraph and the relatively small differences in the predicted translational energy distributions of desorbing H_2O resulting from the direct recombination and kick-out mechanisms (Fig. 1 and 2), it is also possible that prompt recombination is responsible for the T_{trans} = 1800 K component—either alone, or in combination with the kick-out mechanism. As for the T_{trans} = 10 000 K component, it could be formed *via* secondary recombination processes involving photofragments in/on the ice. We cannot decisively rule out any other mechanism in these cases.

The present experimental results support the view that 157 nm irradiation of ASW leads to desorption of H_2O molecules in excited vibrational levels. The H_2O photodesorption results of Öberg *et al.* were interpreted by assuming a dominant role for direct photofragment recombination and subsequent desorption, though these workers could not exclude some contribution from the "kick-out" mechanism.[32] Their results further suggested an increased importance of desorption induced by secondary recombination of photofragments with increasing surface temperature. It is quite likely therefore that we have here been able to show evidence of all three of these photodesorption mechanisms: kick-out, direct recombination, and secondary recombination.

One interesting observation regarding molecules desorbing *via* the kick-out mechanism is that their translational energies are much higher than the rotational energies. The likely explanation for this is that the H atom is released along the hydrogen bond connecting it to the neighboring H_2O molecule. It thereby hits the O atom and not one of the H atoms. The latter encounters might be expected to lead to reaction, or high rotational excitation. If the H atom hits the H_2O close to its center of mass, however, most of the energy will be transferred into translation (rather than rotation). Impacting on the O atom in H_2O will create an intermediate H_3O configuration that would be expected to re-dissociate into H and H_2O, rather than H_2 + OH. Yabushita *et al.*[57,58] have observed desorbing H_2 molecules following UV photoexcitation of ASW, however, which were attributed to reaction of H atoms with H_2O molecules. Because the H_2O molecules in our MD simulations are restricted to be rigid, it is not possible at present to study this reaction. For future simulation studies it would be interesting to allow the molecules to be fully flexible and to study the relative importance of the kick-out mechanism *versus* reaction in H–H_2O collisions. It is also not clear whether the OH radical formed in the H + H_2O reaction will desorb and if, in that case, it would contribute significantly to the observed OH energy distributions and desorption probabilities (see below).

In order to evaluate the limitations of the use of the rigid H_2O model a preliminary study has been performed on H atom–H_2O collisions in the gas phase.[59,60] We have carried out quasi-classical trajectory calculations of the isolated H–H_2O system at different initial H atom kinetic energies (E_i(H) = 1–3 eV) where the H_2O molecules are treated as fully flexible. In total 1000 trajectories have been run. At E_i(H) = 1.5 eV (representative of H atoms released in the ice photodissociation simulations) the resulting vibrational excitation of the target H_2O is on average 0.11 eV. Considering that the lowest vibrational excitation energy possible out of the ground state in a full quantum mechanical treatment of the system is 0.20 eV, this suggests that a large fraction of the H_2O molecules kicked out by H atoms from the ice would indeed not be vibrationally excited—as suggested by the present experiments and MD simulations. The use of the rigid H_2O actually allows us to describe the kick-out of vibrationally cold (v = 0) molecules more realistically by restricting the flow of energy into vibrational modes. Quantum mechanically, no energy whatsoever would be transferred to vibrational modes in this process, but in the classical treatment of flexible molecules any small amount of vibrational energy would be allowed. We thereby approximately take into account the strongly quantized nature of the H_2O vibrations by disallowing vibrational excitations in the kick-out of vibrationally cold molecules, but allowing excitation into the more "classical" rotational and translational degrees of freedom. The obvious limitation of the rigid model has so far been that no estimate of

the probability of vibrational excitation during kick-out has been possible. We hope to provide better estimates of these excitation probabilities in future studies.

5.2 OH photodesorption

The translational energies of the desorbing OH($v = 0$) and OH($v = 1$) products from fresh ASW are best fitted with a temperature $T_{trans} = 1300 \pm 200$ K.[61] This temperature ($\langle E_{trans} \rangle = 0.22 \pm 0.03$ eV) accords well with the 1500 K value reported in the gas phase photodissociation of water at 157 nm by Mikulecky *et al.*,[62] and with the present MD calculations that predict $T_{trans} = 1700 \pm 100$ K for OH($v = 0$) and 1350 ± 150 K for OH($v = 1$). The small (5–10%) contribution of fast ($T_{trans} = 7500$ K) OH products (Table 2) is likely to be due to a secondary photoprocess involving H_2O_2 products on ASW, since the ASW surface used in the present experiments was not completely fresh even with intermissive deposition of fresh water. Since OH photoproducts are readily trapped in the ice matrix, H_2O_2 was produced on the water ice surface at 90 K presumably due to recombination of photolytically produced OH,[61]

$$OH + OH \rightarrow H_2O_2. \quad (4)$$

H_2O_2 formed *via* reaction (4) could be subsequently photodissociated to generate OH as a secondary photoproduct,

$$H_2O_2 + h\upsilon \rightarrow 2OH. \quad (5)$$

The measured rotational temperatures ($T_{rot}(v = 0) = 400$ K and $T_{rot}(v = 1) = 300$ K) are not thermally equilibrated with the ice film temperature of 90 K. The corresponding MD simulations gave $T_{rot}(v = 0) = 480 \pm 50$ K and $T_{rot}(v = 1) = 520 \pm 120$ K, while Mikulecky *et al.*[62] reported $T_{rot}(v = 0) = 620$ K and $T_{rot}(v = 1) = 460$ K for the OH products from the gas phase photodissociation of H_2O. These results suggest that we are observing nascent OH photofragments originating from the ASW surface. This is supported by the MD simulations, where only a small fraction of OH radicals from the top three monolayers can desorb. The lack of a surface accommodated TOF component in the present results indicates that OH formed in the ice bulk are readily trapped or react with water molecules in the ice bulk. In addition, the rotational distribution is essentially the same as those observed and calculated for gas-phase H_2O photolysis. We conclude that the dominant fraction of OH desorbed into vacuum is released from the topmost monolayer(s) of ASW.

The vibrational population distribution ratio measured in the present experiments, $N(v = 1)/N(v = 0) = 0.30 \pm 0.05$, agrees well with the MD predictions ($N(v = 1)/N(v = 0) = 0.24 \pm 0.04$). The fractions of the total available energy partitioned into the different degrees of freedom in the dissociation products have also been determined. From the experimental translational, vibrational, and rotational distributions, we deduce that 8–12% (0.18–0.27 eV) of the available energy ($E_{avl} \sim 2.23$ eV) is partitioned into OH translation, 5–7% (0.11–0.16 eV) into vibration, and 1–2% (0.02–0.04 eV) into rotation. The remainder presumably has been partitioned into the ASW matrix and the translational energy of the H atom. These estimates also agree well with the MD simulations, which suggest that, on average, 26 kJ mol^{-1} is partitioned into OH translation, 12 kJ mol^{-1} into vibration and 6 kJ mol^{-1} into rotation.

The MD calculations predict that the photodesorbed OH would be found in vibrational states up to $v = 6$. OH levels with $v \geq 2$ are predicted to constitute just 10% of the total population, however, with $v = 2$ accounting for some 6% and decreasing percentages in levels with higher v quantum number. Experimentally, we found no evidence for any OH products in levels with $v > 1$. It could be that the populations in such levels are below the present experimental detection limit, or that their relative populations are over-predicted in the MD simulations. Additionally, the assignment and binning of classical trajectories into product vibrational quantum states is also admittedly not well defined, since a continuum of vibrational energies is found in the simulations. However, the good agreement between the experimental and calculated $N(v = 1)/N(v = 0)$ population ratios seems to suggest that the current approach is reasonable.

It is interesting to note the difference between the gas phase and solid phase photodynamics for H_2O at 157 nm. Hwang *et al.*[63] and Yang *et al.*[64] showed that OH($v = 1$) is more populated than OH($v = 0$) in the gas phase photodissociation, but that the OH($v \geq 2$) population is below the detection threshold. This vibrational state distribution is very different from the condensed phase results presented in this paper. Reasons for this can be traced to differences in the excited state potentials, dissipation of energy, and/or the dynamics of the photodissociation process. The two first cases have already been discussed in some depth by Andersson *et al.*[36,37] In short, there is evidence that the surrounding water molecules affect the electronically excited state of H_2O, by lowering the intramolecular part of the excitation energy. The product energy distributions resulting from photoexcitation to such a modified PES would be expected to differ from those formed if the excited molecule was unperturbed by its neighbors. The translational energy distribution of the desorbing H atoms seems to be influenced by this effect, possibly combined with the dissipation of excess energy. This dissipation of energy will most likely proceed through energy transfer to vibrational modes of water molecules in the ice and/or through reaction of energetic H atoms with H_2O.[65]

$$H + H_2O \rightarrow H_2 + OH \quad (6)$$

The good agreement between the classical MD calculations and the experimental results could be fortuitous, but there may be a more fundamental explanation for this accord. In general, full quantum dynamics calculations are required in order to obtain reliable product quantum state distributions—as reported for the photodissociation of gas-phase H_2O molecules by van Harrevelt and van Hemert.[44] In the case of multidimensional systems like a liquid or a solid, however, the most important quantum effects are often "static", *e.g.*, the inclusion of zero-point energy, rather than dynamic interference effects.[66] The reason for this is the rapid loss of coherence that is common in condensed phases. In a low-dimensional quantum system, like a single H_2O molecule, interference effects will be prominent and are likely to have a

significant influence on the product energy distribution. Poulsen and co-workers[66] have demonstrated that it is possible to obtain good agreement with experimental data for different dynamic properties of a range of fluids, including water, by initializing classical dynamics using quantum mechanical initial distributions, the so-called "classical Wigner" approach. This approach is also the basis of the MD calculations presented here, albeit in a somewhat less sophisticated fashion than that used by Poulsen *et al.*[66] We assume that it is sufficient to use a quantum initial distribution only for the intramolecular degrees of freedom of the photoexcited molecule, while the rest of the ice is initiated classically.

6. Summary

We report energy distributions for $H_2O(v = 0)$ molecules and $OH(v = 0,1)$ radicals desorbed following 157 nm photexcitation of amorphous solid water at 90 K. The translational and rotational energy distributions of photodesorbed $H_2O(v = 0)$ molecules measured by REMPI agree well with results from MD simulations on the kick-out mechanism, *i.e.*, desorption induced by momentum transfer from an energetic H atom formed from photodesorption of another H_2O molecule in the ice. The MD simulations also predict another distinct H_2O desorption mechanism, wherein the H and OH fragments formed after excitation and dissociation of a H_2O molecule recombine and subsequently desorb. Whereas the kick-out mechanism mainly leads to desorption of vibrationally cold molecules, this direct recombination mechanism yields highly vibrationally excited molecules. Results from measurements and simulations of the translational and rotational energy distributions of desorbed $OH(v = 0)$ and $OH(v = 1)$ fragments were also in good agreement, as are the relative populations of $OH(v = 1)$ and $OH(v = 0)$. Both the H_2O molecules and the OH radicals are formed translationally hot, but with significantly cooler rotational distributions.

Measured H^+ and OH^+ signals were deduced to originate from desorbing vibrationally excited water molecules. If this is the case, this forms the first experimental evidence of photodesorption of vibrationally excited H_2O from water ice. Two distinct populations were detected, one that appeared promptly and another that grew in relative importance with increasing irradiation time. The former was found to have the same translational temperature as $H_2O(v = 0)$, $T_{trans} = 1800$ K, as well as having a similar translational energy distribution to desorption resulting from the direct desorption mechanism predicted by the MD simulations. It, too, was considered to arise by the kick-out of vibrationally excited H_2O molecules, or by prompt geminate recombination of H and OH photoproducts followed by desorption, or a combination of both mechanisms. The latter population had a much hotter translational temperature, $T_{trans} = 10\,000$ K. The time evolution of this component suggests that it probably arises from the secondary recombination of photoproducts at the surface (since the concentration of photoproduced radicals will increase with irradiation time). In these experiments we might therefore have observed H_2O photodesorption resulting from three distinct mechanisms: kick-out, direct recombination, and secondary recombination.

We hope to extend our comparison between experiments and simulations in future studies. In the MD simulations we aim to make all H_2O molecules fully flexible to allow for the study of energy transfer into and out of vibrational degrees of freedom as well as the reaction of H and H_2O. It would also be very interesting to simulate recombination of thermalized photofragments, H and OH, to predict the behavior of the longer-time secondary processes following photoirradiation. One application would be to estimate the probability of recombination-induced desorption discussed in this paper and the resulting distribution of excess recombination energy. Performing the experiment on solid D_2O could also be illuminating, as the spectroscopy for probing excited vibrational states of D_2O is more promising than for H_2O because of the lower dissociation rates in the C state of D_2O.

Acknowledgements

This work is supported by grants-in-aid from JSPS (Grants No. 20245005 and 23684045). The work by CA was funded by TOP grant No. 700.56.321 by CW/NWO. The MD calculations were performed at Chalmers Center for Computational Science and Engineering (C3SE) computing resources.

References

1 P. Klán and I. Holoubek, *Chemosphere*, 2002, **46**, 1201.
2 B. J. Murray and J. M. C. Plane, *Atmos. Chem. Phys.*, 2005, **5**, 1027.
3 A. G. G. M. Tielens, *The Physics and Chemistry of the Interstellar Medium*, Cambridge University Press, Cambridge, UK, 2005.
4 W. Zheng, D. Jewitt and R. I. Kaiser, *J. Phys. Chem. A*, 2009, **113**, 11174.
5 G. B. Hansen and T. B. McCord, *J. Geophys. Res.*, 2004, **109**, E01012.
6 C. A. Griffith, T. Owen, T. R. Geballe, J. Rayner and P. Rannou, *Science*, 2003, **300**, 628.
7 R. H. Brown, R. N. Clark, B. J. Buratti, D. P. Cruikshank, J. W. Barnes, R. M. E. Mastrapa, J. Bauer, S. Newman, T. Momary, K. H. Baines, G. Bellucci, F. Cappaccioni, P. Cerroni, M. Combes, A. Coradini, P. Drossart, V. Formisano, R. Jaumann, Y. Langevin, D. L. Matson, T. B. McCord, R. M. Nelson, P. D. Nicholson, B. Sicardy and C. Sotin, *Science*, 2006, **311**, 1425.
8 M. E. Brown and W. M. Calvin, *Science*, 2000, **287**, 107.
9 D. C. Jewitt and J. Luu, *Science*, 2004, **432**, 731.
10 K. M. Barkume, M. E. Brown and E. L. Schaller, *Astrophys. J.*, 2006, **640**, L87.
11 C. A. Trujillo, M. E. Brown, K. M. Barkume, E. L. Schaller and D. L. Rabinowitz, *Astrophys. J.*, 2007, **655**, 1172.
12 J. C. Cook, S. J. Desch, T. L. Roush, C. A. Trujillo and T. R. Geballe, *Astrophys. J.*, 2007, **663**, 1406.
13 F. Merlin, A. Guilbert, C. Dumas, M. A. Barucci, C. de Bergh and P. Vernazza, *Astron. Astrophys.*, 2007, **466**, 1185.
14 C. Dumas, B. Carry, D. Hestroffer and F. Merlin, *Astron. Astrophys.*, 2011, **528**, A105.
15 C. A. Trujillo, S. S. Sheppard and E. L. Schaller, *Astrophys. J.*, 2011, **730**, 105.
16 A. C. A. Boogert, T. L. Huard, A. M. Cook, J. E. Chiar, C. Knez, L. Decin, G. A. Blake, A. G. G. M. Tielens and E. F. van Dishoeck, *Astrophys. J.*, 2011, **729**, 92.
17 J. E. Chiar, Y. J. Pendleton, L. J. Allamandola, A. C. A. Boogert, K. Ennico, T. P. Greene, T. R. Geballe, J. V. Keane, C. J. Lada, R. E. Mason, T. L. Roellig, S. A. Sandford, A. G. G. M. Tielens, M. W. Werner, D. C. B. Whittet, L. Decin and K. Eriksson, *Astrophys. J.*, 2011, **731**, 9.
18 K. M. Pontoppidan, E. F. van Dishoeck and E. Dartois, *Astron. Astrophys.*, 2004, **426**, 925.

19 K. M. Pontoppidan, C. P. Dullemond, E. F. van Dishoeck, G. A. Blake, A. C. A. Boogert, N. J. Evans II, J. E. Kessler-Silacci and F. Lahuis, *Astrophys. J.*, 2005, **622**, 463.
20 A. C. A. Boogert, K. M. Pontoppidan, C. Knez, F. Lahuis, J. Kessler-Silacci, E. F. van Dishoeck, G. A. Blake, J.-C. Augerau, S. E. Bisschop, S. Bottinelli, T. Y. Brooke, J. Brown, A. Crapsi, N. J. Evans II, H. J. Fraser, T. L. Huard, J. K. Jørgensen, K. I. Öberg, L. E. Allen, P. M. Harvey, D. W. Koerner, L. G. Mundy, D. L. Padgett, A. I. Sargent and K. R. Stapelfeldt, *Astrophys. J.*, 2008, **678**, 985.
21 G. Zasowski, F. Kemper, D. M. Watson, E. Furlan, C. J. Bohac, C. Hull and J. D. Green, *Astrophys. J.*, 2009, **694**, 459.
22 A. A. Schegerer and S. Wolf, *Astron. Astrophys.*, 2010, **517**, A87.
23 D. Hollenbach, M. J. Kaufman, E. A. Bergin and G. J. Melnick, *Astrophys. J.*, 2009, **690**, 1497.
24 F. F. S. van der Tak, C. M. Walmsley, F. Herpin and C. Ceccarelli, *Astron. Astrophys.*, 2006, **447**, 1011.
25 C. Dominik, C. Ceccarelli, D. Hollenbach and M. Kaufman, *Astrophys. J.*, 2005, **635**, L85.
26 P. H. Hahn, W. G. Schmidt, K. Seino, M. Preuss, F. Bechstedt and J. Bernholc, *Phys. Rev. Lett.*, 2005, **94**, 037404.
27 S. L. Chin, *Phys. Rev. A: At., Mol., Opt. Phys.*, 1971, **4**, 992.
28 H. Rottke, C. Trump and W. Sandner, *J. Phys. B: At., Mol. Opt. Phys.*, 1998, **31**, 1083.
29 D. M. Bartels and R. A. Crowell, *J. Phys. Chem. A*, 2000, **104**, 3349.
30 M. S. Westley, R. A. Baragiola, R. E. Johnson and G. A. Baratta, *Nature*, 1995, **373**, 405.
31 M. S. Westley, R. A. Baragiola, R. E. Johnson and G. A. Baratta, *Planet. Space Sci.*, 1995, **43**, 1311.
32 K. I. Öberg, H. Linnartz, R. Visser and E. F. van Dishoeck, *Astrophys. J.*, 2009, **693**, 1209.
33 T. Hama, A. Yabushita, M. Yokoyama, M. Kawasaki and S. Andersson, *J. Chem. Phys.*, 2009, **131**, 054508.
34 A. Yabushita, T. Hama, M. Yokoyama, S. Andersson, R. N. Dixon, M. N. R. Ashfold and N. Watanabe, *Astrophys. J.*, 2009, **699**, L80.
35 T. Hama, M. Yokoyama, A. Yabushita, M. Kawasaki, S. Andersson, M. N. R. Ashfold, C. M. Western and N. Watanabe, *J. Chem. Phys.*, 2010, **132**, 164508.
36 S. Andersson, A. Al-Halabi, G. J. Kroes and E. F. van Dishoeck, *J. Chem. Phys.*, 2006, **124**, 064715.
37 S. Andersson and E. F. van Dishoeck, *Astron. Astrophys.*, 2008, **491**, 907.
38 C. Arasa, S. Andersson, H. M. Cuppen, E. F. van Dishoeck and G. J. Kroes, *J. Chem. Phys.*, 2010, **132**, 184510.
39 A. Al-Halabi, E. F. van Dishoeck and G. J. Kroes, *J. Chem. Phys.*, 2004, **120**, 3358.
40 A. Al-Halabi, H. J. Fraser, G. J. Kroes and E. F. van Dishoeck, *Astron. Astrophys.*, 2004, **422**, 777.
41 W. L. Jorgensen, J. Chandrasekhar, J. D. Madura, R. W. Impey and M. L. Klein, *J. Chem. Phys.*, 1983, **79**, 926.
42 A. J. Dobbyn and P. J. Knowles, unpublished.
43 F. J. Aoiz, L. Bañares, J. F. Castillo, M. Brouard, W. Denzer, C. Vallance, P. Honvault, J.-M. Launay, A. J. Dobbyn and P. J. Knowles, *Phys. Rev. Lett.*, 2001, **86**, 1729.
44 R. van Harrevelt and M. C. van Hemert, *J. Chem. Phys.*, 2001, **114**, 9453.
45 K. Kobayashi, *J. Phys. Chem.*, 1983, **87**, 4317.
46 A. Yabushita, Y. Inoue, T. Senga, M. Kawasaki and S. Sato, *J. Phys. Chem. B*, 2002, **106**, 3151.
47 S. Sato, D. Yamaguchi, K. Nakagawa, Y. Inoue, A. Yabushita and M. Kawasaki, *Langmuir*, 2000, **16**, 9533.
48 M. E. Greenslade, M. I. Lester, D. C. Radenovic, A. J. A. van Roij and D. H. Parker, *J. Chem. Phys.*, 2005, **123**, 074309.
49 F. M. Zimmermann and W. Ho, *Surf. Sci. Rep.*, 1995, **22**, 127.
50 C.-H. Yang, G. Sarma, J. J. ter Meulen, D. H. Parker and C. M. Western, *Phys. Chem. Chem. Phys.*, 2010, **12**, 13983.
51 M. N. R. Ashfold, J. M. Bayley, R. N. Dixon and J. D. Prince, *Ber. Bunsenges. Phys. Chem.*, 1985, **89**, 254 and references therein.
52 H. Dickinson, S. R. Mackenzie and T. P. Softley, *Phys. Chem. Chem. Phys.*, 2000, **2**, 4669.
53 M. N. R. Ashfold, J. M. Bayley and R. N. Dixon, *Chem. Phys.*, 1984, **84**, 35.
54 B. W. Uselman, J. M. Boyle and S. L. Anderson, *Chem. Phys. Lett.*, 2007, **440**, 171.
55 C. M. Western, *PGOPHER, a Program for Simulating Rotational Structure*, University of Bristol, available at http://pgopher.chm.bris.ac.uk.
56 A. G. Sage, T. A. A. Oliver, R. N. Dixon and M. N. R. Ashfold, *Mol. Phys.*, 2010, **108**, 945 and references therein.
57 A. Yabushita, T. Hama, D. Iida, N. Kawanaka, M. Kawasaki, N. Watanabe, M. N. R. Ashfold and H.-P. Loock, *Astrophys. J.*, 2008, **682**, L69.
58 A. Yabushita, T. Hama, D. Iida, N. Kawanaka, M. Kawasaki, N. Watanabe, M. N. R. Ashfold and H.-P. Loock, *J. Chem. Phys.*, 2008, **129**, 044501.
59 C. Arasa, S. Andersson, H. M. Cuppen, E. F. van Dishoeck and G. J. Kroes, *J. Chem. Phys.*, 2011, **134**, 164503.
60 C. Arasa, M. C. van Hemert, E. F. van Dishoeck, G. J. Kroes, in preparation.
61 A. Yabushita, T. Hama, D. Iida and M. Kawasaki, *J. Chem. Phys.*, 2008, **129**, 014709.
62 K. Mikulecky, K. H. Gericke and F. J. Comes, *Chem. Phys. Lett.*, 1991, **182**, 290.
63 D. W. Hwang, X. F. Yang and X. M. Yang, *J. Chem. Phys.*, 1999, **110**, 4119.
64 X. F. Yang, D. W. Hwang, J. J. Lin and X. Ying, *J. Chem. Phys.*, 2000, **113**, 10597.
65 A. Yabushita, D. Kanda, N. Kawanaka, M. Kawasaki and M. N. R. Ashfold, *J. Chem. Phys.*, 2006, **125**, 133406.
66 J. A. Poulsen, G. Nyman and P. J. Rossky, *Proc. Natl. Acad. Sci. U. S. A.*, 2005, **102**, 6709.

